



Inverse correlation of fluctuations of cerebral blood and water concentrations in humans

Viola Borchardt^{1,a} , Vesa Korhonen^{1,2} , Heta Helakari^{1,2} ,
Maiken Nedergaard^{3,4} , Teemu Myllylä^{1,5} , Vesa Kiviniemi^{1,2,6,b}

¹ Oulu Functional Neuroimaging Group, Research Unit of Medical Imaging Physics and Technology (MIPT), University of Oulu, Oulu, Finland

² Department of Diagnostic Radiology, Medical Research Center (MRC), Oulu University Hospital, Oulu, Finland

³ Center for Translational Neuromedicine, University of Copenhagen, Copenhagen, Denmark

⁴ Center for Basic and Translational Neuroscience, Faculty of Health and Medical Sciences, University of Copenhagen, Copenhagen, Denmark

⁵ Optoelectronics and Measurement Techniques Research Unit, University of Oulu, Oulu, Finland

⁶ Present address: Department of Diagnostic Radiology, P.O. Box 50, 90029 Oulu, OYS, Finland

Received: 24 October 2020 / Accepted: 22 April 2021

© The Author(s) 2021

Abstract Near-infrared spectroscopy (fNIRS) measures concentrations of oxygenated (HbO) and deoxygenated (HbR) hemoglobin in the brain. Recently, we demonstrated its potential also for measuring concentrations of cerebral water (cH₂O). We performed fNIRS measurements during rest to study fluctuations in concentrations of cH₂O, HbO and HbR in 33 well-rested healthy control subjects (HC) and 18 acutely sleep-deprived HC. Resting-state fNIRS signal was filtered in full-band, cardiac, respiratory, low-, and very-low-frequency bands. The sum of HbO and HbR constitutes the regional cerebral blood volume (CBV). CBV and cH₂O concentrations were analyzed via temporal correlation and phase synchrony. Fluctuation in concentrations of cH₂O and CBV was strongly anti-correlated across all frequency bands in both frontal and parietal cortices. Fluctuation in concentrations of cH₂O and CBV showed neither a completely synchronous nor a random phase relationship in both frontal and parietal cortices. Acutely sleep-deprived subjects did not show significant differences in temporal correlation or phase synchrony between fluctuations in cH₂O and CBV concentrations compared with well-rested HC. The reciprocal interrelation between fluctuations in CBV and cH₂O concentrations is consistent with the Munro–Kellie doctrine of constant intracranial volume. This coupling may constitute a functional mechanism underlying glymphatic circulation, which persists despite acutely disturbed sleep patterns.

Focus Point on Breakthrough Optics- and Complex Systems-based Technologies of Modulation of Drainage and Clearing Functions of the Brain.

^a e-mail: borchardt.viola@googlemail.com (corresponding author)

^b e-mail: vesa.kiviniemi@oulu.fi

1 Introduction

Upon neuronal activation, increases in the oxygenated hemoglobin (HbO) concentration within the blood vasculature are accompanied by reciprocal decreases in deoxygenated hemoglobin (HbR) concentration [1]. This hemodynamic response is the basis for inferences about brain function in several neuroimaging techniques, notably the blood oxygenation level dependent (BOLD) MR signal. An alternative technique called functional near-infrared spectroscopy (fNIRS) is based on light injection and detection on the scalp and reveals fluctuations in both HbO and HbR concentrations within a cortical sampling volume [2–5]. The sum of HbO and HbR constitutes the regional cerebral blood volume (CBV), which represents a surrogate index for altered neuronal activity in brain tissue [6]. The CBV signal may present a steady time course, but the constituent HbO and HbR signals are typically anticorrelated [7], with the direction of change in CBV matching that of HbO. On the other hand, the HbR concentration is determined by venous blood oxygenation, which is strongly modulated by vasodilation driven by the neuronal tissue [8,9]. Furthermore, cerebral blood flow in gray matter depends on sleep/wake stage, suggesting a mechanism controlling cerebral circulation [10].

Much like blood, cerebrospinal fluid (CSF) comprises 10% of the volume within the human cranium [11]. CSF consists of 99% water, is continuously produced in the choroid plexus, and flows through the ventricles and the basal cisterns to the subarachnoid space [12,13]. Fluid production at the choroid plexus is thought to create a pressure gradient that determines the direction of net fluid flow, but CSF circulation is also driven by factors such as arterial pulsatility, respiratory venous fluctuations, and slow vasomotion. CSF flow samples the brain interstitial fluid and eliminates macroscopic neurotoxic waste products such as degraded proteins, other metabolites, or electrolytes from the brain [14]. This clearance process is the core function of the intracerebral bulk flow, now known as the “glymphatic system” [15].

In the context of the glymphatic system theory, investigation of CSF dynamics has attracted increasing interest. Obtaining parameters that characterize cerebral fluid flow dynamics and define driving forces of fluid flow in the human brain is a necessary key for understanding glymphatic system function and dysfunction. This need accounts for the emergence of non-invasive approaches to simultaneously measure the concentration changes of cerebral water (cH_2O), HbO, and HbR in humans [16,17].

A recent study by Myllylä et al. demonstrated the possibility to sense dynamic variations of cH_2O in human using technique based on fNIRS [16]. The changes in brain water signal, measured by fNIRS, are affected by both dynamics of CSF and blood-bound water. As presented in this study, the effect of blood-bound water in cH_2O signal can be reduced when volume of blood is measured and supposed that concentration changes of blood-bound water in blood vessels are negligible when compared to volume changes in CSF. Unraveling the interrelation of fluctuations in CBV and cH_2O concentrations is a fundamental step to gaining better understanding of the mechanisms of fluid dynamics and their interactions in the human brain.

The Munro–Kellie doctrine states that, since the skull is a rigid, confined compartment with a constant intracranial volume, any change in fluid concentration or pressure needs to be counterbalanced to maintain volume equilibrium [18]. In other words, the sum of the volumes of brain matter, CSF, and blood must be constant. A more current and comprehensive view on the Munro–Kellie doctrine includes the whole central nervous system and considers the spinal cord as a viscoelastic extension of the brain. In each cardiac cycle, pulsatile brain deformations driven by physiological pulsations are being relayed on to the ventricles, forc-

ing CSF displacement from the confined cranium back and forth into the spinal canal [19]. However, due to fundamental reversed anatomical positioning and viscoelastic differences, mean diffusion and convective transport of CSF in gray and white matter are likely to differ between brain and spinal cord [20]. In healthy humans, brain matter is considered to have a fairly constant volume. Although some oscillations in cerebral tissue occur due to cardiovascular and vasomotor pulsations [21], blood and CSF are the major intracranial volume buffers.

Thus, we hypothesized that concentrations of CBV and cH_2O would exhibit (1) temporal fluctuations and (2) possibly a counteracting relationship. Furthermore, recent advances have differentiated endogenous brain activity fluctuations that originate from different physiological sources [21,22]. We therefore expected that fNIRS measures would exhibit oscillations in the physiological frequency bands, which previously have been shown to drive CSF pulsations. To test these linked hypotheses, we used fNIRS to measure the relationships between fluctuations in hemoglobin and cH_2O concentrations in 33 well-rested healthy subjects.

Intriguingly, the glymphatic system is mainly disengaged during wakefulness and is activated during sleep or anesthesia [23–26]. Accumulating evidence suggests that sleep disruption interferes with glymphatic clearance and ultimately increases the risk of developing neurodegenerative diseases [24,26–30]. Furthermore, sleep efficiency in patients with cerebrovascular diseases correlates inversely with the volume of the perivascular Virchow–Robin spaces, which are the main channels for glymphatic flow [31]. Given this background, perturbation of normal sleep pattern would affect cerebral fluid interactions in an awake resting state. To test this hypothesis, we studied influences of acute sleep deprivation in 18 healthy subjects after a night without sleep. We supposed that any perturbations in the interrelation of CBV and cH_2O concentrations in sleep deprivation states would be more pronounced in well-rested subjects than in acute sleep deprivation.

2 Methods

2.1 Subjects

Two groups of participants were recruited: 33 well-rested healthy control subjects (HC, 15 females, mean age \pm standard deviation (s.d.): 29.7 ± 8.1 years) and 18 healthy subjects performing one night of sleep deprivation (longitudinal design, a subset of the 33 HC, 8 females, mean age: 29.7 ± 6.5 years). Mann–Whitney U test showed no significant difference in age ($p > 0.05$). Subjects were recruited from the general population by advertisement and screened for absence of neurological disorders, major cardiovascular or respiratory diseases, continuous medication, drug abuse, and shift work. Written informed consent was obtained from each participant prior to testing, in accordance with the Declaration of Helsinki (1983). The regional Ethical Committee of Northern Ostrobothnia Hospital District in Oulu University Hospital approved the study protocols.

2.2 Experimental design

Our custom-made MRI-compatible fNIRS using four wavelengths (660 nm, 740 nm, 830 nm, 980 nm) is presented in [16]. In this device, four NIRS channels were mounted on a DC electroencephalography (EEG) cap with 256 electrodes (manufactured by Electrical Geodesic Incorporation, USA). Two channels were positioned on the left forehead above the eyebrow around the Fp1 electrode (according to the international 10–20 system used for EEG)

and the other two on the mid parietal cortex near the Pz electrode. The distances between light source and long-range detector and between light source and short-range detector were 3–3.5 cm and 1–1.5 cm, respectively. Optodes were fixed in place with adhesive tape, and a black spacer protected the eyes from laser reflections.

Subjects assumed a supine position in a 3 Tesla MRI scanner and were asked to lie still, think of nothing specific, and fixate their eyes on a cross displayed on a screen. Hearing was protected via earplugs, and head motion was minimized using soft pads fitted over the ears. For all participants, resting-state fNIRS was measured for 10 min. Well-rested HC were measured in the afternoon. For the sleep-deprivation condition, some of the HC subjects repeated the measurement in the early morning after one night without sleep. During this measurement, the room was not illuminated, and subjects could keep their eyes closed.

2.3 fNIRS device and measurements

fNIRS allows the detection of various chemical components of biological tissue based on the absorbance and scattering of light by organic molecules. Light is projected on the tissue, and the back-scattered light at wavelengths ranging from 650 to 1000 nm can be recorded when using high-sensitive photodetectors for detailed qualitative spectroscopic analysis of chemical structures in the brain. Conventional fNIRS devices usually use two wavelengths to measure blood-flow-related changes in hemoglobin saturation, more precisely HbO and HbR.

Modifications in this technique enable measurement of other chromophores in the human tissue, for example cytochrome oxidase, fat, or water [32,33]. An isosbestic point corresponds to a specific wavelength at which the absorption spectra of two chromophores cross each other and thus have equal absorbance. To quantify concentrations of two chromophores, it is advisable to select two wavelengths on both sides of the respective isosbestic point, whereas three or more wavelengths are required for the measurement of three chromophores. In this study, we measured HbO, HbR, and water concentrations. We selected 660 nm and 830 nm, thus to either side of the isosbestic point (800 nm) of the HbO and HbR absorption spectrum [34]. We chose 980 nm to probe water activity, since the isosbestic point for water and HbO is approximately at 930 nm [35,36]. To correct for the respective photosensitivity of each optode, the light intensities were multiplied with the wavelength-dependent photosensitivity.

We note that the measured water signal is potentially comprised of intracellular and extracellular compartments in the measurement volume underneath the optodes. However, intracellular water is not expected to display significant fluctuations in concentration during a 10-min measurement in a resting subject. Dynamics in the calculated water signal are therefore assumed to be caused by the composite concentration changes in CSF and blood-bound water, here referred to as cerebral water (cH₂O).

The additional short-range fNIRS sensor captured mainly dynamics from skin and skull due to its lower penetration depth. Since water and hemoglobin are not thought to cause significant signal fluctuations in skin and skull, the short-range sensor captured extracerebral artifacts and its signal were used to improve quality of the long-range signal [37].

In total, 102 fNIRS datasets were acquired (33 well-rested and 18 acutely sleep-deprived, each in two cortical regions). The raw fNIRS signals were visually inspected to assure quality. In case of a saturated signal or large artifacts, the corrupted part of the signal was removed and only the artifact-free part was used for analysis. The minimum length of signal recordings was 5 min. Four datasets were excluded (two of the well-rested HC and two of the sleep-deprived group due to malfunctioning frontal laser). After completing two-thirds of the measurements,

the frontal laser failed and had to be replaced with a laser at 940 nm that was available at that time.

2.4 fNIRS data processing

Raw fNIRS optical intensities were converted into time courses representing concentration fluctuations based on the modified Beer–Lambert law [38–40]. The following extinction coefficients were used: for 660nm: HbR: 3.4408, HbO: 0.3346, H₂O: 0.0166; for 830 nm: HbR: 0.7804, HbO: 1.0507, H₂O: 0.1459; for 940 nm: HbR: 0.7874, HbO: 1.3520, H₂O: 0.8804; and for 980 nm: HbR: 0.4233, HbO: 1.2513, H₂O: 2.1491 [41]. The differential path length factor was 5.93 [42]. Distances measured between optodes were used in each individual calculation. Calculated mean concentrations for HbR, HbO, and cH₂O reflect the total measurement volume underneath the optode.

The time course of signals from the short-range skin detector was subtracted from that of long-range detector to improve detection of signal dynamics in deeper cortical layers [43]. The remaining dynamics in the signals are attributable to physiological events occurring below the skull layer. All signals were separately despiked using interpolation [44], linearly detrended, and low-pass filtered at 0–5 Hz. Total hemoglobin concentration (HbT, equivalent to CBV representing a surrogate index for neuronal activity) was derived by adding HbR and HbO concentrations. To account for differences in signal amplitudes between subjects, the signals were scaled in the range of [0, 1]. Time courses were additionally band-pass-filtered into four physiological frequency bands, which have been the focus of several previous fNIRS studies [45]: the cardiac band (0.7–1.5 Hz), the respiratory band (0.12–0.4 Hz), the range of low-frequency fluctuations (0.01–0.1 Hz), and very-low-frequency fluctuations (0.001–0.01 Hz).

2.5 Data analysis and statistical analysis

Frontal and parietal measurements were considered separately because they are independent datasets. All calculations were performed in MATLAB R2017b. fNIRS data from well-rested HC were used to replicate the previously established relationships between HbO, HbR, and CBV. To investigate the relationships between hemoglobin and cH₂O, the CBV signals were pairwise-correlated in time with the cH₂O signals.

Correlations between fluctuations in CBV and cH₂O concentrations were calculated in five frequency bands. Group differences between well-rested and sleep-deprived HC in the temporal relationship between amplitude fluctuations in cH₂O and CBV concentrations were calculated using two-sample *t* tests.

Phase synchrony between CBV and cH₂O signals was estimated by calculating the phase-locking value (PLV) based on cardiac, respiratory, and low-frequency bands, because estimation of phase-synchrony requires a filtered signal [46]. PLV is a measure of consistency of phase differences of two signals at a given frequency, where the phase component is obtained separately from the amplitude component. PLV has values in the range of [0 1], where unity represents absolute phase synchrony. A Hilbert transform was used to compute phases of the signals using customized code from the NBT toolbox ([47], RRID: SCR_009612). PLV was calculated in a sliding-window manner with an overlap of 75% between windows. The length of the windows was adapted to the respective frequency band (window length for cardiac band: 2 s; respiratory band: 10 s; low-frequencies: 120 s). For each band, the PLVs were averaged across windows to obtain an optimal compromise between statistical accuracy and stationarity.

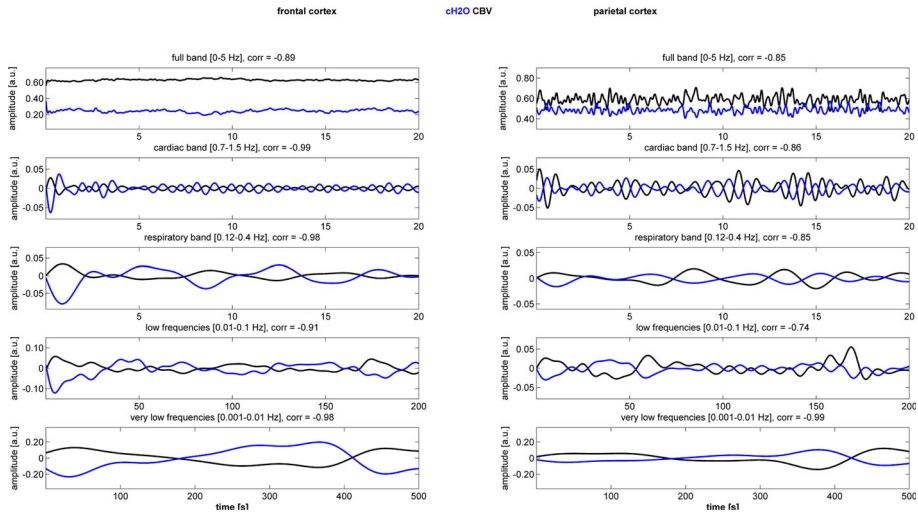


Fig. 1 Filtered fNIRS signals of cerebral water (blue, cH₂O) and total cerebral blood volume (black, CBV) concentrations in five frequency bands in both frontal (left panel) and parietal (right panel) cortices depicted for one exemplary well-rested healthy subject. Individual correlation coefficients between temporal fluctuations in cH₂O and CBV are given in the title of each subplot

Intra-individual variation was assessed by calculating the absolute difference in correlation coefficients as well as PLV between conditions and paired *t*-tests were used to compare the intra-individual variations in correlation of cH₂O and CBV.

3 Results

3.1 Relationship between cerebral water and blood volume in well-rested subjects

We initially inspected the signals of CBV and cH₂O on a single subject level (Fig. 1). CBV and cH₂O concentrations exhibited opposing time courses in both cortical locations and across all frequency bands.

We replicated previously established relationships between HbO, HbR, and CBV in the group of well-rested HC subjects (Fig. 2). As expected, fluctuations in HbO and CBV concentrations were strongly correlated (frontal cortex: mean = 0.88 ± 0.32 , parietal cortex: mean = 0.79 ± 0.38), while the relationship between HbR and HbO showed moderate anti-correlations (frontal cortex: mean = -0.37 ± 0.51 , parietal cortex: mean = -0.47 ± 0.46). Fluctuations in HbR and CBV concentration were uncorrelated (frontal cortex: mean = -0.08 ± 0.55 , parietal cortex: mean = -0.06 ± 0.54). The temporal relationship between amplitude fluctuations in cH₂O and CBV concentrations revealed strong anti-correlations (frontal cortex: mean = -0.76 ± 0.24 , parietal cortex: mean = -0.72 ± 0.28).

The anti-correlations between amplitude fluctuations in cH₂O and CBV concentrations were present also in cardiac (frontal cortex: mean = -0.53 ± 0.46 , parietal cortex: mean = -0.76 ± 0.31), respiratory (frontal cortex: mean = -0.66 ± 0.30 , parietal cortex: mean = -0.75 ± 0.27), low-frequency (frontal cortex: mean = -0.77 ± 0.25 , parietal cortex: mean = -0.67 ± 0.39), and very-low-frequency bands (frontal cortex: mean = -0.80 ± 0.22 , parietal cortex: mean = -0.60 ± 0.43 , Fig. 3).

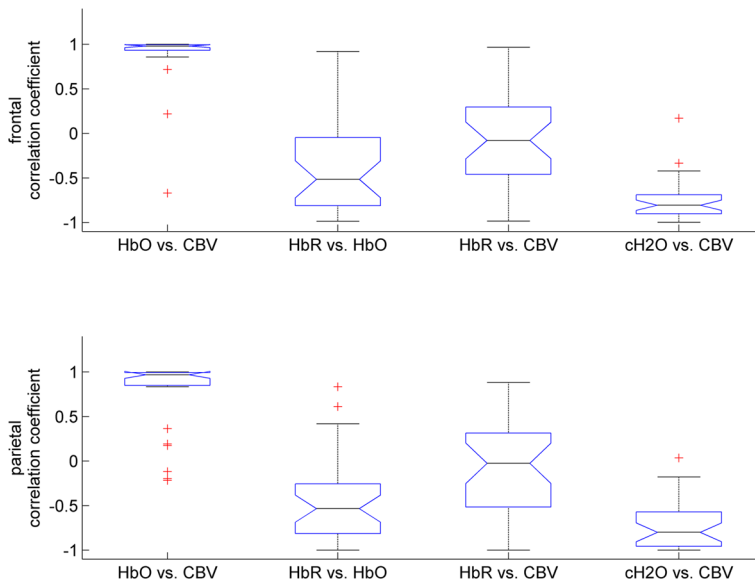


Fig. 2 Correlations between fluctuations in hemoglobin and cerebral water concentrations in both frontal and parietal cortices in the full-band (0–5 Hz) in healthy well-rested subjects. On each box, the central line indicates the median, and the bottom and top edges indicate the 25th and 75th percentiles, respectively. The whiskers extend to the most extreme data points and outliers are plotted as red crosses. HbO: oxygenated hemoglobin, HbR: deoxygenated hemoglobin

Next, we investigated phase synchrony between CBV and cH_2O across cardiac, respiratory, and low-frequency bands. CBV and cH_2O concentrations had median phase locking values reflecting neither a completely synchronous nor a random relationship and were similar for frontal and parietal cortices (Fig. 4). Phase synchrony between CBV and cH_2O concentrations was constant across frequency bands (frontal cortex: cardiac: mean = 0.57 ± 0.22 , respiratory: mean = 0.58 ± 0.18 , low frequencies: mean = 0.62 ± 0.17 ; parietal cortex: cardiac: mean = 0.68 ± 0.20 , respiratory: mean = 0.66 ± 0.18 , low frequencies: mean = 0.59 ± 0.24 , Fig. 4).

3.2 Effect of acute sleep deprivation on relationship between cerebral water and hemoglobin

To investigate the effect of acute sleep deprivation on the relationship between cH_2O and CBV concentrations, individual correlation coefficients were compared between the well-rested and acutely sleep-deprived states.

Also in the sleep-deprived state, the temporal relationship between amplitude fluctuations in cH_2O and CBV concentrations revealed anti-correlations (frontal cortex: mean = -0.57 ± 0.40 , parietal cortex: mean = -0.66 ± 0.37 , Fig. 5). Group differences between well-rested and sleep-deprived HC in the temporal relationship between amplitude fluctuations in cH_2O and CBV concentrations were not significantly altered (frontal cortex: $p = 0.052$, parietal cortex: $p = 0.63$). Subjects showed variations in their individual direction of change, i.e., increases or decreases, from well-rested to acutely sleep-deprived state. However, a significant effect of acute sleep deprivation in intra-individual variations between cH_2O and CBV concentrations was not found (all $p > 0.05$, Table 1).

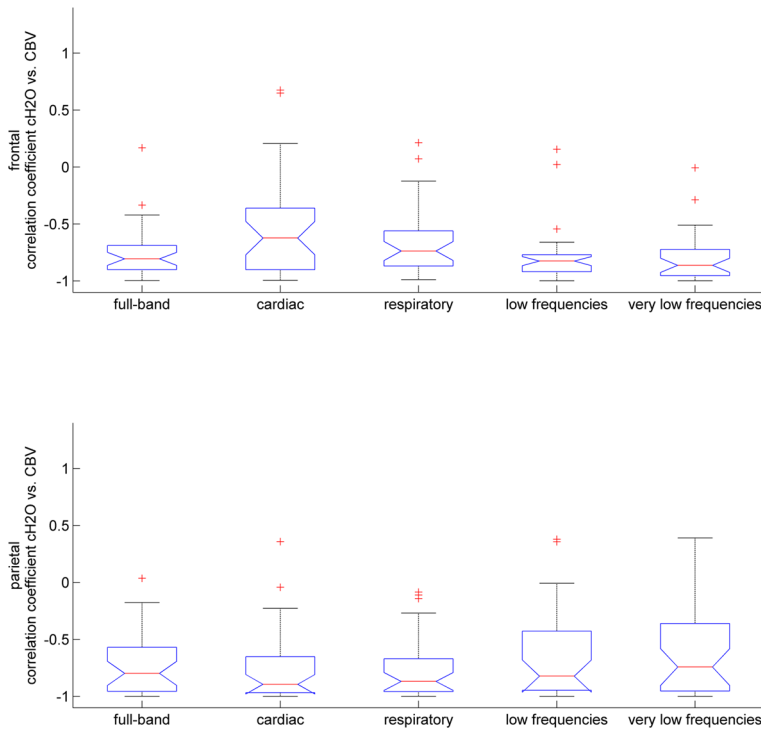


Fig. 3 Correlations between fluctuation in cerebral water (cH_2O) and cerebral blood volume (CBV) concentrations in five physiological frequency bands in both frontal (upper panel) and parietal cortices (lower panel) in well-rested healthy subjects. On each box, the central line indicates the median, and the bottom and top edges indicate the 25th and 75th percentiles, respectively. The whiskers extend to the most extreme data points and outliers are plotted as black crosses. CBV: cerebral blood volume; cH_2O : cerebral water

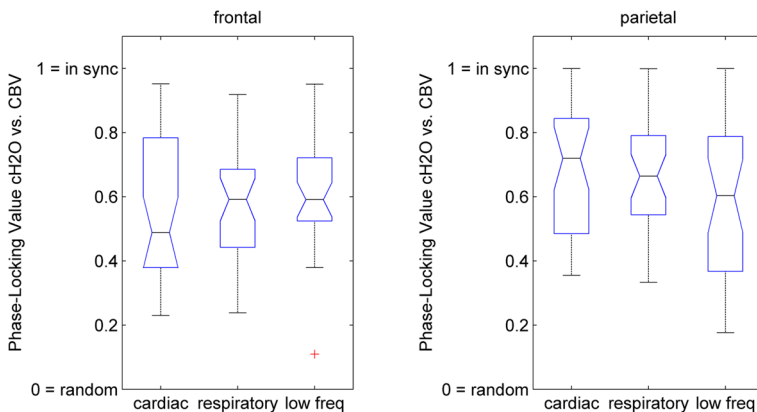


Fig. 4 Phase synchrony of fluctuations between cerebral water (cH_2O) and cerebral blood volume (CBV) in three physiological frequency bands (cardiac band (0.7–1.5 Hz), respiratory band (0.12–0.4 Hz), low-frequency fluctuations (0.01–0.1 Hz)) in both frontal and parietal cortices in well-rested healthy subjects. On each box, the central line indicates the median, and the bottom and top edges indicate the 25th and 75th percentiles, respectively. The whiskers extend to the most extreme data points and outliers are plotted as black crosses

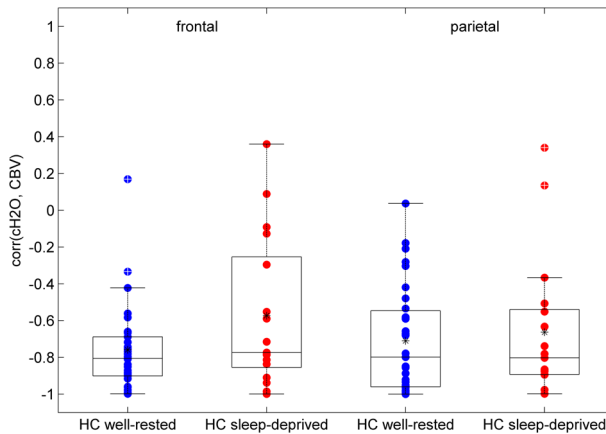


Fig. 5 Effects of acute sleep deprivation on temporal correlation between cerebral water (cH_2O) and cerebral blood volume (CBV) in the full frequency band (0–5 Hz) in both frontal and parietal cortices. Every colored circle represents data from one subject (blue: well-rested subjects, red: acutely sleep-deprived subjects). On each box, the central line indicates the median, the black star the mean, and the bottom and top edges indicate the 25th and 75th percentiles, respectively. The whiskers extend to the most extreme data points and outliers are plotted as white crosses

Table 1 Intra-individual variation expressed as absolute difference ($|\Delta|$) in correlation coefficient and results of paired t tests between well-rested versus acutely sleep-deprived states in HC subjects in five frequency bands and both frontal and parietal cortices

$ \Delta\text{corr}(\text{cH}_2\text{O}, \text{CBV}) $, p value of paired t test					
	Full-band	Cardiac	Respiratory	Low frequencies	Very low frequencies
Frontal	5.22, $p = 0.18$	6.70, $p = 0.39$	6.89, $p = 0.51$	4.23, $p = 0.37$	4.64, $p = 0.30$
Parietal	4.53, $p = 0.76$	4.54, $p = 0.38$	4.64, $p = 0.56$	7.90, $p = 0.99$	7.51, $p = 0.037$

Table 2 Intra-individual variation expressed as absolute difference ($|\Delta|$) in PLV and results of paired t tests between well-rested versus acutely sleep-deprived states in HC subjects in five frequency bands and both frontal and parietal cortices

$ \Delta\text{PLV}(\text{cH}_2\text{O}, \text{CBV}) $, p value of paired t test			
	Cardiac	Respiratory	Low frequencies
Frontal	4.14, $p = 0.84$	3.72, $p = 0.91$	4.37, $p = 0.50$
Parietal	3.26, $p = 0.46$	2.71, $p = 0.67$	4.29, $p = 0.88$

Subjects showed individual variations (i.e., increases or decreases) in their PLV between well-rested and acutely sleep-deprived states (Table 2), but no significant effects of acute sleep deprivation on intra-individual variations between cH_2O and CBV concentrations were observed across cardiac, respiratory and low-frequency bands (all $p > 0.05$, Table 2).

4 Discussion

The presented results are significant in at least two major aspects and in consequence with the previously shown findings presented in [16]. This is the first report of non-invasively measured fluctuations in the concentration of cH_2O in the human brain, entailing a total of 102 human datasets to provide robust statistical inferences. Second, our inferences on relation between CBV and cH_2O were drawn based on two cortical locations, which showed similar patterns. The most interesting finding that fNIRS measurements revealed is that fluctuations in cH_2O concentration in the human brain were strongly anti-correlated with CBV across five physiological frequency bands. There was no evidence for phase synchrony between cH_2O and CBV concentrations, as PLVs consistently fell between absolute synchrony and randomness, which indicates that their time courses were out of phase across the five frequency bands.

Acutely sleep-deprived subjects did not show significant differences in the interrelation of cH_2O and CBV when compared to well-rested healthy subjects, during resting-state measurement. However, HC subjects with acute sleep deprivation showed high intra-individual variability in the direction of change in the correlation, indicating a heterogeneous response to acute sleep deprivation across subjects.

These present observations are difficult to compare to the first presentation of concentration levels of cH_2O (Figure 7 in [16]), because the subject in that study had been examined in sitting position with the fNIRS channel placed on the occiput. In that study, the fNIRS cerebral water signal showed a positive correlation with the blood oxygen level-dependent (BOLD) signal measured using functional magnetic resonance imaging (fMRI) [16]. There is no previous research utilizing fNIRS to study the interaction of cH_2O and CBV.

In light of the Munro–Kellie doctrine, we expected an anticorrelation between amplitude fluctuations in the concentration of CBV and cH_2O , which are together the major buffers in the cranial compartment. The doctrine assumes that the brain matter is incompressible and has a constant volume in healthy humans [18]. If the concentration of one constituent increases in a space of fixed volume, the concentration of another constituent must necessarily decrease to maintain volume equilibrium. Given the long-known anti-correlation between HbO and HbR concentrations, one could expect opposing relationships with cH_2O . As known from the fMRI BOLD literature [8], local neuronal activity entails hyperemia and dilation of arteries and veins containing relatively more oxygenated blood. At the same time, concentrations of cerebral water and HbR are substituted. Upon neuronal deactivation, the venous volume declines, thus increasing the HbR concentration. In this situation, the available space is filled with CSF, thus raising and thereby re-establishing cH_2O . This scenario predicts for an anti-correlation with cH_2O , as depicted schematically in Fig. 6.

CBV did not show phase synchrony with cH_2O , which indicates that these signals do not engage in direct oscillatory coupling with a preferred phase difference. This might exclude any functional relevance of their phase relationship. Alternatively, there may be relationships that are not fully uncovered by the measures employed in this study. Relevant information might be hidden in dynamic lag structures, and it is conceivable that dynamic alterations might exist in water exchange between different CSF compartments of the whole central nervous system, i.e., spinal and intracranial spaces [48]. For example, the venous blood compartment has been considered to have a balloon effect during activation-driven increases in blood flow [8]. Also, in contrast to the skull, the venous structures around the spinal canal are not surrounded by bones and may therefore enable a markedly stronger cushioning effect compared to intra-cranial veins. This cushioning effect may well alter the time domain signals measured by NIRS in a nonlinear dynamic way, which can make direct time signal

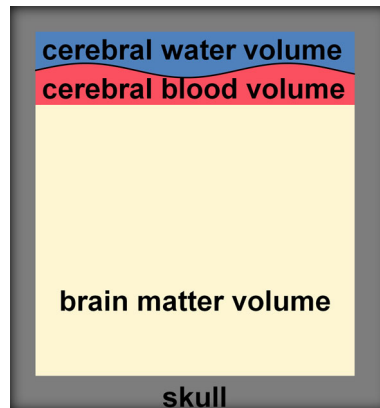


Fig. 6 Schematic representation of the observed relationships in the context of the Munro–Kellie doctrine. The skull frames a confined space, which is 80% filled with incompressible brain matter, and with 10% volume fraction for blood and cerebrospinal fluid. If the volume within the skull is constant [18], any change in component volume or concentration is met by a change to maintain equilibrium. Cerebral blood volume (CBV) comprises the sum of oxygenated (HbO) and deoxygenated hemoglobin (HbR) concentrations. CBV and cerebral water volume functionally counteract, which is depicted by the curved line representing opposite fluctuations in concentrations of CBV and cH_2O at physiological frequencies measured using non-invasive fNIRS

correlations with constant lag difficult. Furthermore, the spinal canal CSF siphoning of flow is likely to add another source of delay into the correlation analysis. Further multimodal studies to assess these signals during execution of cognitive, affective, or sensory tasks should help resolve this issue.

The observed relationships between CBV and cH_2O concentrations were similar in all tested physiological frequency bands, hinting towards the absence of specific influences of any frequency range. Therefore, it seems that the interrelation between CBV and cH_2O is not driven by any specific oscillation frequency. This observation is consistent with previous evidence for a contribution of these physiological frequencies to glymphatic pulsation mechanisms [21].

A previous fNIRS study showed that one night of sleep deprivation in healthy subjects reduced the wavelet-based phase coherence between left and right prefrontal oxyhemoglobin oscillations [49]. Another fNIRS study on phase and amplitude of oscillatory components of cerebral hemodynamics during sleep in human subjects showed that blood volume and flow velocity oscillations maintained their relative phase difference during sleep, although their amplitudes were attenuated during non-REM sleep [45]. If sleep disruption indeed altered the coupling pattern in our subjects, we might have expected a higher correlation between fluctuations in cH_2O and CBV. But the interrelation showed a stable pattern despite acute sleep deprivation, albeit of higher variance. Whether deep sleep alters the observed correlation/anticorrelation patterns remains a question for future research requiring measurements performed also during sleep.

Of note, the novelty of our methodology calls for caution in the interpretation of our results. For example, the analyzed cH_2O signal may consist of intracellular and extracellular (containing interstitial fluid, CSF, and blood plasma) water compartments in the cortical area underneath the optode. However, these affect mainly the DC level of the measured signals. Thus, shown cH_2O dynamics are assumed to be caused by concentration changes in CSF, interstitial fluid, and blood-bound water. Due to the current limitations in the spatial

resolution of fNIRS, it is not possible to localize the exact source of the signal contributing to the cH_2O concentration. Currently, validation studies for the method are conducted using animal models. For instance, an animal model utilizing thinned skull technique, the similar measurements can be repeated in the absence of light penetrance problems in extracerebral layers.

We emphasize that our present fNIRS methods do not measure whole-brain water content, which are 80–85% (w/v) in adults [50]. While the brain water content is higher and shows a high variability in infants due to physiological maturation processes and flexibility in the presence of open fontanels, it is nearly constant in adults [51,52]. With fNIRS, the absolute concentration changes in hemoglobin cannot be quantified, and the precise correlation between the fNIRS signal and neural activity remains to be fully understood [2]. These reservations notwithstanding, our present data processing pipeline included removal of artifactual signals from extracerebral tissue as suggested by [37], which greatly improved signal quality and increases the validity of derived inferences. Interregional comparisons of NIRS signal amplitudes are not as reliable as those of hemodynamic changes, because of its vulnerability to spatial variation in skull and subarachnoidal space thickness [53,54].

The present repeated fNIRS measurements in HC subjects had small variations in optode positioning between the two acquisitions, which would result in uncertainty regarding signal localization. However, since the analysis of the relation between cH_2O and CBV with high temporal resolution is the main interest of this study, the exact positioning of the optodes is less of an issue.

In this experimental arm of a larger multimodal assessment of brain function, subjects were measured while lying in an MRI scanner. Since a third of subjects likely fall asleep within 3 min of resting-state fMRI studies [55], it is likely that vigilance declined during the measurements in our subjects. Especially for the cases of sleep-deprived HC subjects, we cannot exclude possible interference of light sleep intervals. A detailed evaluation of sleep stages is outside the scope of the current work. Since fNIRS supports essentially unlimited measurement time, future studies may investigate possible effects on vigilance fluctuations on the functional interrelation between cH_2O and CBV fluctuations based on 24-hour measurements during normal sleep, sleep deprivation, or sleep restriction, and pharmacofNIRS.

The current approach could be applied for clinical research in other patient datasets, for example in Alzheimer's dementia patients, in whom disrupted sleep architecture and glymphatic failure may contribute to neurodegeneration [56]. Indeed, recent glymphatic research showed reduced CSF pressure in patients suffering from Alzheimer's disease [19], which could predict for altered relationships between cerebral water and CBV. Another interesting clinical relationship is intracranial pressure changes occurring in patients with so-called normal pressure hydrocephalus. However, measurement of intracranial pressure is invasive and hence not advisable in healthy volunteers.

Based on the previous proof-of-concept study, we show that fNIRS measurements of cH_2O and CBV are technically feasible in patients. No study has hitherto supported an analysis of fluctuations in cerebral water concentration. The observed anti-correlation between CBV and cH_2O may constitute a fundamental functional mechanism underlying glymphatic circulation in the human brain.

Funding Open access funding provided by University of Oulu including Oulu University Hospital. Funding was provided by Academy of Finland (Grant No. 314502).

Open Access This article is licensed under a Creative Commons Attribution 4.0 International License, which permits use, sharing, adaptation, distribution and reproduction in any medium or format, as long as you give appropriate credit to the original author(s) and the source, provide a link to the Creative Commons licence,

and indicate if changes were made. The images or other third party material in this article are included in the article's Creative Commons licence, unless indicated otherwise in a credit line to the material. If material is not included in the article's Creative Commons licence and your intended use is not permitted by statutory regulation or exceeds the permitted use, you will need to obtain permission directly from the copyright holder. To view a copy of this licence, visit <http://creativecommons.org/licenses/by/4.0/>.

References

1. M. Ferrari, V. Quaresima, *Neuroimage* **63**, 921–935 (2012)
2. Y. Hoshi, *Philos. Trans. R. Soc. A Math. Phys. Eng. Sci.* **369**, 4407–4424 (2011)
3. M. Strait, M. Scheutz, *Front. Neurosci.* **8**, 117 (2014)
4. R.C. Mesquita, M.A. Franceschini, D.A. Boas, *Biomed. Opt. Express* **1**, 324–336 (2010)
5. F. Jobsis, *Science* **198**, 1264–1267 (1977)
6. L. Gagnon, R.J. Cooper, M.A. Yücel, K.L. Perdue, D.N. Greve, D.A. Boas, *Neuroimage* **59**, 2518–2528 (2012)
7. A. Kleinschmidt, H. Obrig, M. Requardt, K.-D. Merboldt, U. Dirnagl, A. Villringer, J. Frahm, J. Cereb. Blood Flow Metab. **16**, 817–826 (1996)
8. R.B. Buxton, E.C. Wong, L.R. Frank, *Magn. Reson. Med.* **39**, 855–864 (1998)
9. C.N. Hall, C. Reynell, B. Gesslein, N.B. Hamilton, *Nature* **508**, 55–60 (2014)
10. R.E. Townsend, P.N. Prinz, W.D. Obrist, J. Appl. Physiol. **35**, 620–625 (1973)
11. A. Thrane, V. Thrane, M. Nedergaard, *Trends Neurosci.* **36**, 52–60 (2009)
12. R. Spector, R.F. Keep, S. Robert Snodgrass, Q.R. Smith, C.E. Johanson, *Exp. Neurol.* **267**, 78–86 (2015)
13. D. Orešković, M. Radoš, M. Klarica, *Neuroscience* **354**, 69–87 (2017)
14. S. Dreha-Kulaczewski, A.A. Joseph, K.-D. Merboldt, H.-C. Ludwig, J. Gartner, J. Frahm, J. Neurosci. **35**, 2485–2491 (2015)
15. M. Nedergaard, *Science* **340**, 1529–1530 (2013)
16. T. Myllylä, E. Vihriälä, M. Pedone, V. Korhonen, L. Surazynski, M. Wróbel, A. Zienkiewicz, J. Hakala, H. Sorvoja, J. Lauri, T. Fabritius, M. Jędrzejewska-Szczerska, V. Kiviniemi, I. Meglinski, in *Proc. SPIE 10063, Dyn. Fluctuations Biomed. Photonics XIV* (2017)
17. T. Myllylä, M. Harju, V. Korhonen, A. Bykov, V. Kiviniemi, I. Meglinski, J. Biophotonics **11**, e201700123 (2018)
18. B. Mokri, *Neurology* **56**, 1746–1748 (2001)
19. A.A. Linninger, M. Xenos, B. Sweetman, S. Ponskshe, X. Guo, R. Penn, J. Math. Biol. **59**, 729–759 (2009)
20. S. Liu, M.A. Lam, A. Sial, S.J. Hemley, L.E. Bilston, M.A. Stoodley, *Fluids Barriers CNS* **15**, 13 (2018)
21. V. Kiviniemi, X. Wang, V. Korhonen, T. Keinänen, T. Tuovinen, J. Autio, P. LeVan, S. Keilholz, Y.-F. Zang, J. Hennig, M. Nedergaard, J. Cereb. Blood Flow Metab. **36**, 1033–1045 (2015)
22. J.J. Iliff, H. Lee, M. Yu, T. Feng, J. Logan, M. Nedergaard, H. Benveniste, J. Clin. Investig. **123**, 1299–1309 (2013)
23. L. Xie, H. Kang, Q. Xu, M.J. Chen, Y. Liao, M. Thiagarajan, J.O. Donnell, D.J. Christensen, J.J. Iliff, T. Takano, R. Deane, M. Nedergaard, *Science* **342**, 373–7 (2013)
24. S. Ooms, S. Overeem, K. Besse, M.O. Rikkert, M. Verbeek, J.A.H.R. Claassen, *JAMA Neurol.* **71**, 971–977 (2014)
25. E.L. Boespflug, J.J. Iliff, *Biol. Psychiatry* **83**, 328–336 (2017)
26. E. Shokri-Kojori, G.-J. Wang, C.E. Wiers, S.B. Demiral, M. Guo, S.W. Kim, E. Lindgren, V. Ramirez, A. Zehra, C. Freeman, G. Miller, P. Manza, T. Srivastava, S. De Santi, D. Tomasi, H. Benveniste, N.D. Volkow, *Proc. Natl. Acad. Sci.* **115**, 4483–4488 (2018)
27. C.R. Kyrtos, J.S. Baras, in *BIOTECHNO 2014: The Sixth International Conference on Bioinformatics, Biocomputational Systems and Biotechnologies* (2014)
28. G. Ringstad, K.-A. Mardal, P.K. Eide, *JCI Insight* **3**, e121537 (2018)
29. R.O. Weller, E. Djuanda, H.-Y. Yow, R.O. Carare, *Acta Neuropathol.* **117**, 1–14 (2008)
30. J.J. Iliff, M. Wang, Y. Liao, B.A. Plog, W. Peng, G.A. Gundersen, H. Benveniste, G.E. Vates, R. Deane, S.A. Goldman, E.A. Nagelhus, M. Nedergaard, *Sci. Transl. Med.* **4**, 147ra111 (2012)
31. C. Berezuk, J. Ramirez, F. Gao, C.J.M. Scott, M. Huroy, R.H. Swartz, B.J. Murray, S.E. Black, M.I. Boulous, *Sleep* **38**, 853–858 (2015)
32. A. Corlu, R. Choe, T. Durduran, K. Lee, M. Schweiger, S.R. Arridge, E.M.C. Hillman, A.G. Yodh, *Appl. Opt.* **44**, 1948–1956 (2005)
33. V. Tuchin, *Tissue Optics: Light Scattering Methods and Instruments for Medical Diagnosis* (SPIE Optical Engineering Press, Bellingham, 2007), p. 988

34. T. Myllylä, V. Korhonen, V. Kiviniemi, V. Tuchin, in *Proc. SPIE Optical Techniques in Neurosurgery, Neurophotonics, and Optogenetics II* **9305** (2015)
35. M.A. McIntosh, U. Shahani, R.G. Boulton, D.L. McCulloch, *Investig. Ophthalmol. Vis. Sci.* **51**, 2266–2273 (2010)
36. V. Tuchin, *Tissue Optics, Light Scattering Methods and Instruments for Medical Diagnostics* (SPIE PRESS, Bellingham, 2015)
37. L. Gagnon, M.A. Yücel, M. Dehaes, R.J. Cooper, K.L. Perdue, J. Selb, T.J. Huppert, R.D. Hoge, D.A. Boas, *Neuroimage* **59**, 3128–3138 (2012)
38. M. Cope, *Near-Infrared Spectroscopy, Applied Aspects of Ultrasonography in Humans* (InTech, London, 2012), p. 190
39. D.A. Boas, T. Gaudette, G. Strangman, X. Cheng, J.J.A. Marota, J.B. Mandeville, *Neuroimage* **13**, 76–90 (2001)
40. G.E. Strangman, V. Iivkovic, Q. Zhang, J. Appl. Physiol. Jpn. **2**, 124 (2017)
41. P. Van der Zee, M. Cope, S. Arridge, M. Essenpreis, L. Potter, A. Edwards, J. Wyatt, D. McCormick, S. Roth, E. Reynolds, *Adv. Exp. Med. Biol.* **316**, 143–153 (1992)
42. M. Cope, The application of near infrared spectroscopy to non invasive monitoring of cerebral oxygenation in the newborn infant. Ph.D. thesis (1991)
43. L. Gagnon, M.A. Yücel, D.A. Boas, R.J. Cooper, *Neuroimage* **85**, 6–27 (2014)
44. N. Mori, T. Suzuki, S. Kakuno, J. Eng. Mech. **133**, 122–127 (2007)
45. M.L. Pierro, A. Sassaroli, P.R. Bergethon, B.L. Ehrenberg, S. Fantini, *Neuroimage* **63**, 1571–1584 (2012)
46. F. Varela, J. Lachaux, E. Rodriguez, J. Martinerie, *Nat. Rev. Neurosci.* **2**, 229–239 (2001)
47. S.-S. Poil, *Neurophysiological Biomarkers of Cognitive Decline: From Criticality to Toolbox*. Ph.D. thesis, Free University of Amsterdam (2013)
48. M.A. Lam, S.J. Hemley, E. Najafi, N.G.F. Vella, L.E. Bilston, M.A. Stoodley, *Sci. Rep.* **7**, 12924 (2017)
49. L. Bu, M. Zhang, J. Li, F. Li, H. Liu, Z. Li, *PLoS ONE* **12**, e0177321 (2017)
50. J. Dobbing, J. Sands, *Arch. Dis. Child.* **48**, 757–767 (1973)
51. M. Wolf, G. Naulaers, F. Van Bel, S. Kleiser, G. Greisen, J. Near Infrared Spectrosc. **20**, 43–55 (2012)
52. A. Demel, M. Wolf, C.F. Poets, A.R. Franz, *BMC Pediatr.* **14**, 1–6 (2014)
53. S. Wang, N. Shibahara, D. Kuramashi, S. Okawa, N. Kakuta, E. Okada, A. Maki, Y. Yamada, *Opt. Rev.* **17**, 410 (2010)
54. Y. Hoshi, *Progress in Brain Research: Hemodynamic Signals in FNIRS* (Elsevier, Amsterdam, 2016), pp. 153–179
55. E. Tagliazucchi, H. Laufs, *Neuron* **82**, 695–708 (2014)
56. H. Benveniste, X. Liu, S. Koundal, S. Sanggaard, H. Lee, J. Wardlaw, *Gerontology* **06519**, 1–14 (2018)